
Article:

Chapman, S. C., McIntosh, S. W., Leamon, R. J. and Watkins, N. W. ORCID: 0000-0003-4484-6588 (2020) Quantifying the solar cycle modulation of extreme space weather. Geophysical Research Letters, 47 (11). ISSN 0094-8276

https://doi.org/10.1029/2020GL087795

Geophysical Research Letters

RESEARCH LETTER
10.1029/2020GL087795

Key Points:
- New Sun clock maps solar cycles onto a regular time base quantifying the occurrence times of quiet intervals of each cycle
- 1-3% of severe ($aa > 300$ nT) geomagnetic storms and 4–6% of C-, M-, and X-class solar flares occurred in solar cycle quiet intervals
- Solar cycle modulation of the chance of severe ($aa > 300$ nT) geomagnetic storms is much stronger than that of moderate ($aa > 100$ nT) storms

Supporting Information:
- Supporting Information S1

Correspondence to:
S. C. Chapman,
S.C.Chapman@warwick.ac.uk

Citation:
Chapman S.C., McIntosh, S. W., Leamon, R. J., & Watkins, N. W. (2020). Quantifying the solar cycle modulation of extreme space weather. *Geophysical Research Letters*, *47*, e2020GL087795. https://doi.org/10.1029/2020GL087795

Received 3 MAR 2020
Accepted 21 MAY 2020
Accepted article online 30 MAY 2020

Quantifying the Solar Cycle Modulation of Extreme Space Weather

S. C. Chapman[1], S. W. McIntosh[2], R. J. Leamon[3,4], and N. W. Watkins[1,5,6]

[1]Centre for Fusion, Space and Astrophysics, Physics Department,University of Warwick,Coventry,UK, [2]National Center for Atmospheric Research,Boulder,CO,USA, [3]Department of Astronomy,University of Maryland,College Park,MD,USA, [4]NASA Goddard Space Flight Center, Code 672,Greenbelt,MD,USA, [5]Centre for the Analysis of Time Series,London School of Economics and Political Science,London,UK, [6]Faculty of Science, Technology, Engineering and Mathematics,The Open University,Milton Keynes,UK

Abstract By obtaining the analytic signal of daily sunspot numbers since 1818 we construct a new solar cycle phase clock that maps each of the last 18 solar cycles onto a single normalized 11 year epoch. This clock orders solar coronal activity and extremes of the *aa* index, which tracks geomagnetic storms at the Earth's surface over the last 14 solar cycles. We identify geomagnetically quiet intervals that are 40% of the normalized cycle, $\pm 2\pi/5$ in phase or ± 2.2 years around solar minimum. Since 1868 only two severe ($aa > 300$ nT) and one extreme ($aa > 500$ nT) geomagnetic storms occurred in quiet intervals; 1–3% of severe ($aa > 300$ nT) geomagnetic storms and 4–6% of C-, M-, and X-class solar flares occurred in quiet intervals. This provides quantitative support to planning resilience against space weather impacts since only a few percent of all severe storms occur in quiet intervals and their start and end times are quantifiable.

Plain Language Summary Extreme space weather events or superstorms have a high impact over a wide range of systems, from power supplies, aviation, satellites, and radio communications to economic and social behavior. They are becoming increasingly important as our society relies more and more on being interconnected. While it is well known that severe space weather activity is modulated by the solar cycle, the variable duration of the cycle has made this risk difficult to quantify and there is still the possibility of a severe event during solar minimum. Quantifying the relative likelihood of severe space weather events at different phases of the solar cycle is a key result of this work. We map this irregular cycle in time onto a uniform solar cycle clock and find a quite strong solar cycle modulation, with only a few percent of the most severe solar flares and space storms occurring during the minimum quiet interval of the cycle, the timing of which we have identified. This has operational implications for the users of near-Earth space as well as power grid operators who need to schedule critical maintenance during periods of quiet space weather.

1. Introduction

Extreme space weather events can disrupt power distribution, aviation, communication, and satellites. They are driven by large-scale plasma structures emitted from the solar corona, but the geoeffectiveness of an event depends on many factors, including how the event propagates from Sun to Earth and how it interacts with Earth's magnetosphere (Baker & Lanzerotti, 2016; Hathaway, 2015; Yermolaev et al., 2013). Events that lead to geomagnetically induced currents that affect power grids are statistically more likely close to a solar maximum and in the descending phase of the solar cycle, but importantly they also occur at all other times in the solar activity cycle (Hayakawa et al., 2020; Thomson et al., 2010). As the largest events can result in significant societal impact and financial loss (Hapgood, 2019; Oughton et al., 2017), quantifying the chance of occurrence of extreme space weather events is essential to planning the resilience of vulnerable systems to catastrophic failure.

When more frequent, moderate space weather storms are aggregated across different solar cycles, there is a well-established correlation between occurrence rate and solar cycle modulated activity (Tsubouchi & Omura, 2007; Tsurutani et al., 2006). However, due to their rarity, the likelihood of more extreme geomagnetic storms is challenging to quantify and thus most estimates (Thomson et al., 2011) average over

multiple solar cycles. Estimates based on extrapolating a power law event distribution (Riley, 2012) suggest a 12% probability of a "Carrington-class" (Tsurutani et al., 2003) extreme event in the next solar cycle, but are highly uncertain, and an underlying solar cycle modulation contributes to this uncertainty (Riley & Love, 2016). Some estimates based on extreme value statistics (Thomson et al., 2011) suggest much lower probabilities (Elvidge & Angling, 2018; Silbergleit, 1996, 1999; Siscoe, 1976; Tsubouchi & Omura, 2007).

Crucially, each solar cycle is unique in amplitude and duration (see, e.g., Hathaway, 2015; Russell et al., 2019) and geomagnetic activity tracks the different levels of activity of each solar maximum and declining phase (Chapman, Watkins et al. 2018; Lockwood et al., 2018). Quantifying how solar coronal activity, and the chance of an extreme space weather event, varies within and between solar cycles is central to space weather resilience planning. A uniform normalized time base for the solar cycle is needed in order to collate data across solar cycles of different duration in order to quantify correlation between the frequency of occurrence of severe geomagnetic storms and solar cycle activity phase. In this letter we propose a new solar cycle "clock" that stretches (or shrinks) the observed sunspot cycle of activity onto a single (normalized 11 year) time base. Once we have shown that this clock can be constructed, we find a sharp demarcation between active and quiet intervals of both the level of solar coronal activity and severe geomagnetic activity. We then obtain quantitative estimates of the solar cycle variation in the chance of occurrence of severe and moderate space weather events.

2. Constructing the Solar Cycle Clock

The daily sunspot number record provides an almost uninterrupted measure of solar coronal activity since 1818 and is plotted in Figure 1a. Both the amplitude and duration of each solar cycle varies from one cycle to the next. We express this time series $S(t)$ in terms of a time-varying amplitude $A(t)$ and phase $\varphi(t)$ by obtaining its analytic signal (Boashash, 1992; Gabor, 1946) $A(t)\exp[i\varphi(t)]$ such that the real part of this signal is $S(t)$ and the imaginary part is obtained such that $A(t)\exp[i\varphi(t)] = S(t) + iH(t)$ where $H(t)$ is the Hilbert transform of $S(t)$. This is a standard approach that is used to test for synchronization (e.g., Chapman, Lang, et al. 2018) and for amplitude-frequency relationships (Palŭs & Notovná, 1999). Here it is used to provide a mapping between time and signal phase that converts the (variable) duration of each solar cycle into a corresponding uniform phase interval, from 0 to 2π. We use a standard method to obtain the discrete analytic signal (Marple, 1999) which satisfies both invertability and orthogonality. While defined for an arbitrary time series, the analytic signal will only give a physically meaningful decomposition of the original time series if the instantaneous frequency $\omega(t)=d\varphi(t)/dt$ remains positive (Boashash, 1992). We therefore need to remove fast fluctuations and, for a positive definite signal such as the daily sunspot number, a background trend (see, e.g., Boashash, 1992; Chapman, Lang et al. 2018). Before performing the Hilbert transform we performed a 180 day moving average and obtained a slowly varying trend by performing a robust local linear regression which down weights outliers ("rlowess") using a T_B=*40* year window. Figure 1 charts how we construct the analytic signal for the daily sunspot record. We first subtract the long-timescale trend (blue line in Figure 1a) to give a sunspot time series that is unambiguously zero crossing (Figure 1b). We then obtain the Hilbert transform $H(t)$ for this (T_s = 180 day moving average) smoothed and detrended signal which then gives the analytic signal. Figures 1c and 1d plot $A(t)$ and $\varphi(t)$, respectively. Each cycle maximum (red circles) and minimum (green circles) is also overplotted on the analytic phase. The analytic phase $\varphi(t)$ plotted in Figure 1d will be used to read across between phase φ and occurrence time t. This read-across is robust across a reasonable range of T_s and T_B, for example, the zero crossing times $\varphi(t)$=0 vary by less than ±3 months when calculated over the range T_s = [150–360] days and T_B = [20–80] years. We used the most recent sunspot record, Sunspot Index and Long-term Solar Observations (SILSO) version 2.0 released in 2015 to determine $\varphi(t)$ for this study. There are differences in the way that sunspot records from different eras are combined (see, e.g., Lockwood, Owens, Barnard, Scott, Lockwood et al., 2016; Lockwood, Owens, Barnard, & Usoskin, 2016, and references therein). We have verified that our results are insensitive to this by repeating our analysis using the archived SILSO version 1.0; we find that the zero crossing times $\varphi(t) = 0$ differ at most by less than 2 months.

The times of cycle terminators (McIntosh et al., 2019) are also plotted in Figure 1d (blue circles). They are located between each solar cycle minimum and the maximum of the next cycle, and we set zero phase to be that of the average of the terminators as estimated by McIntosh et al. (2019). Cycle terminators (McIntosh & Leamon, 2014, 2014,2019) have been identified based on multiple observations of coronal magnetic activity

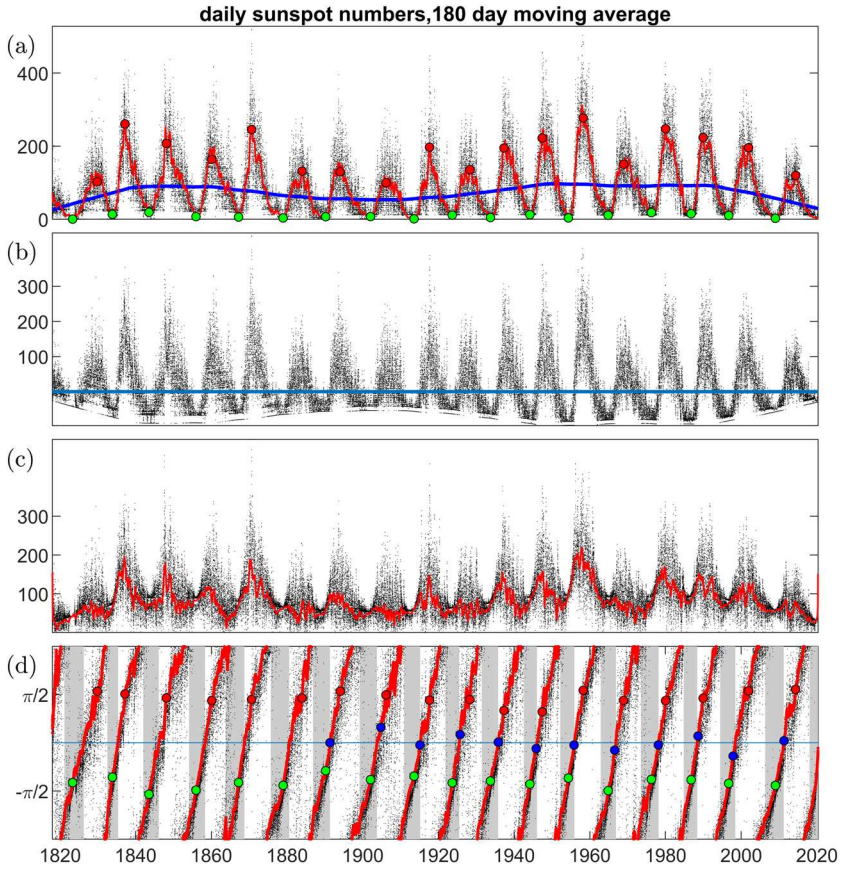

Figure 1. From top to bottom (a) daily sunspot number (black), 180 day moving average (red), and slow timescale trend obtained by local regression on a 40 year window (blue); (b) daily sunspot number with local regression trend subtracted; (c) analytic signal amplitude of daily (black) and moving average (red) sunspot number; (d) analytic signal phase as in (c). The maxima and minima of the last 18 solar cycles are indicated by red and green circles, respectively, and the blue circles indicate terminators for the last 12 solar cycles from McIntosh et al. (2019). Zero phase is set to be at the average phase of the terminators, and the range of phases $[-4\pi/5\ 0]$ are indicated in gray on panel (d); these are the quiet intervals of each cycle.

which indicate the end of one cycle of activity and the beginning of the next. The termination of a solar cycle, or terminator, has a three-component global signature (McIntosh et al., 2019). It is initially observed as a very abrupt reduction in the density of extreme ultraviolet bright point density around the solar equator, marking the final cancelation of the old cycle's (magnetic) activity bands at the equator (McIntosh & Leamon, 2014). The equatorial reduction occurs in close conjunction with a very rapid growth of bright point density in the (magnetic) activity bands at midlatitudes. This switch in magnetic flux emergence patterns occurs at the same time as the rapid increase in the number of midlatitude sunspots which belong to the new solar cycle. At higher solar latitudes, the terminator is signaled as the start of the polar magnetic reversal process (McIntosh et al., 2019) or the "rush to the poles" phenomenon (Babcock, 1961; Sheeley et al., 1989). We may therefore expect terminators to feature in how solar cycle activity is ordered.

We can use the mapping between time and phase shown in Figure 1d to construct a Sun clock which for each solar cycle has a different duration in time, but which maps onto a regular $0–2\pi$ interval in phase. We will see how this orders observations that are available over multiple solar cycles. The F10.7 index (solar radio flux at 10.7 cm Tapping, 2013) is available since 1947 giving six solar cycles of observations. As well as providing an index of the state of the solar corona, it is used by many operational space weather models as their prime solar input. It is correlated with the density of the upper atmosphere which in turn has consequences for the design and operation of satellites in low Earth orbit (e.g., Vedder & Tabor, 1992). The intensity and occurrence times of solar flares seen in X-ray have been continuously observed by GOES, and these are cataloged since 1975, that is, over the last four solar cycles. The intensities of space weather events are routinely characterized by geomagnetic indices derived from ground-based magnetometer observations. The *aa* index

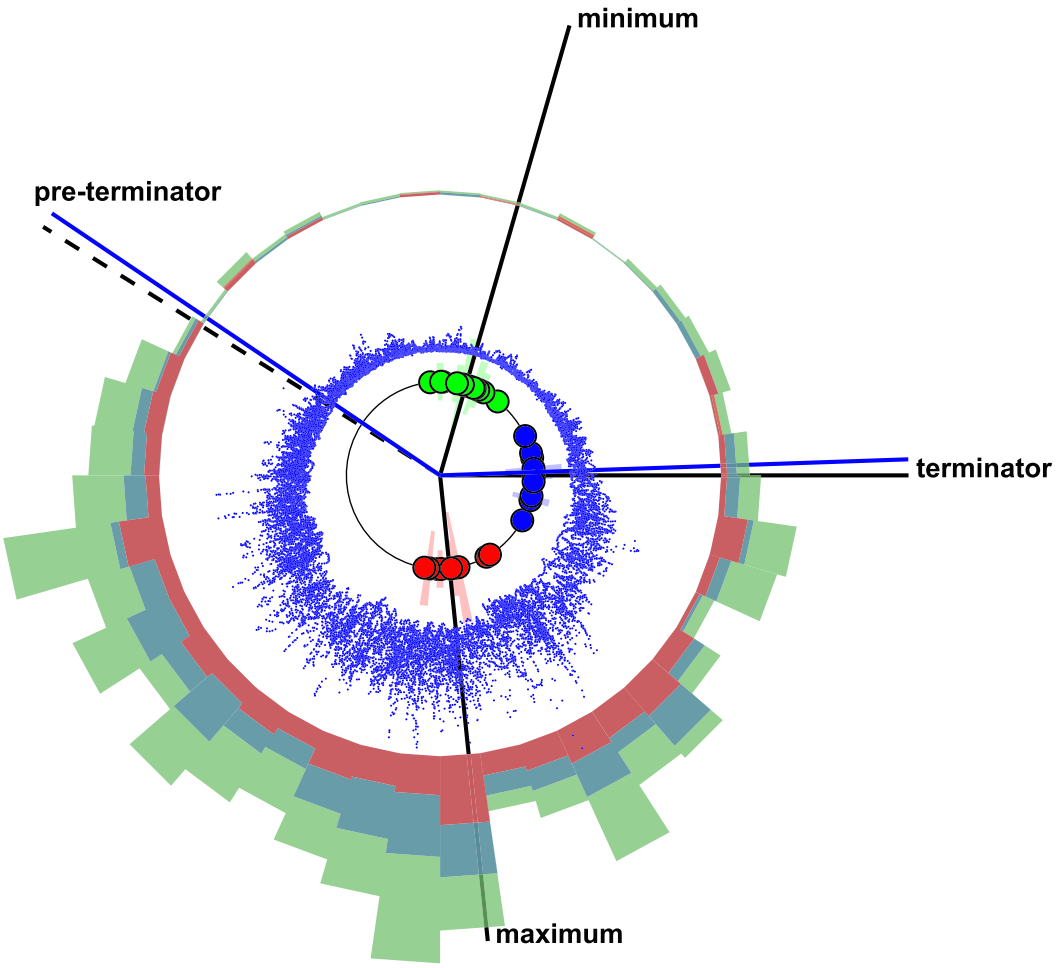

Figure 2. Solar cycle clock constructed such that increasing time (analytic phase) is read clockwise. The analytic phases of the maxima and minima of the last 18 solar cycles are indicated by red and green circles, respectively, and the blue circles indicate terminators for the last 12 solar cycles (McIntosh et al., 2019). Black lines indicate the average analytic phase for the maxima, minima, and terminators. The pre-terminator (dashed black line) is at the same phase difference (clock angle) in advance of the minimum as that phase difference by which the terminator lags the minimum. These phase differences are close to $\pm 2\pi/5$ either side of the average minimum phase; these are indicated by blue lines. Blue dots overplot daily F10.7 and overplotted red, blue, and green histograms show counts in nonoverlapping (normalized) 3-month-long bins for X-class, M-class, and C-class flare occurrence (scaled relative to each other in ratio 75:500:2,000).

is constructed (Mayaud, 1972; 1980) from the 3-hourly K indices determined at two antipodal observatories (invariant magnetic latitude 50°) and is available over the last 14 solar cycles, from 1868 to the present. An important consideration is that the *aa* index (units, nT) is discretized in amplitude (Bubenik & Fraser-Smith, 1977; Chapman et al., 2020) since the underlying K index (Bartels et al., 1939) is a quasi-logarithmic 0–9 integer scale that characterizes the maximum positive and negative magnetic deviations that occur during each 3 hr period at a given observatory.

3. Sun Clocks for Solar and Geomagnetic Activity

We map the last 18 solar cycles onto a regular $[0\ 2\pi]$ interval in phase to produce a clock as shown in Figures 2 and 3. On the inner ring of both figures we plot the minima and maxima of the last 18 cycles and the terminators of the last 12 cycles. Lines indicate the average of each of these; this forms the basis of the solar cycle clock which we can read off as having a (normalized) 11 year period corresponding to 2π in phase. Increasing time (phase) is read clockwise as plotted. We now add to this clock multi-solar cycle observations of solar and geomagnetic activity. Solar flares (cataloged from GOES X-ray flux observations) occurrence is plotted as (scaled) counts in nonoverlapping (normalized) 3 month binned histograms in Figure 2, X-class,

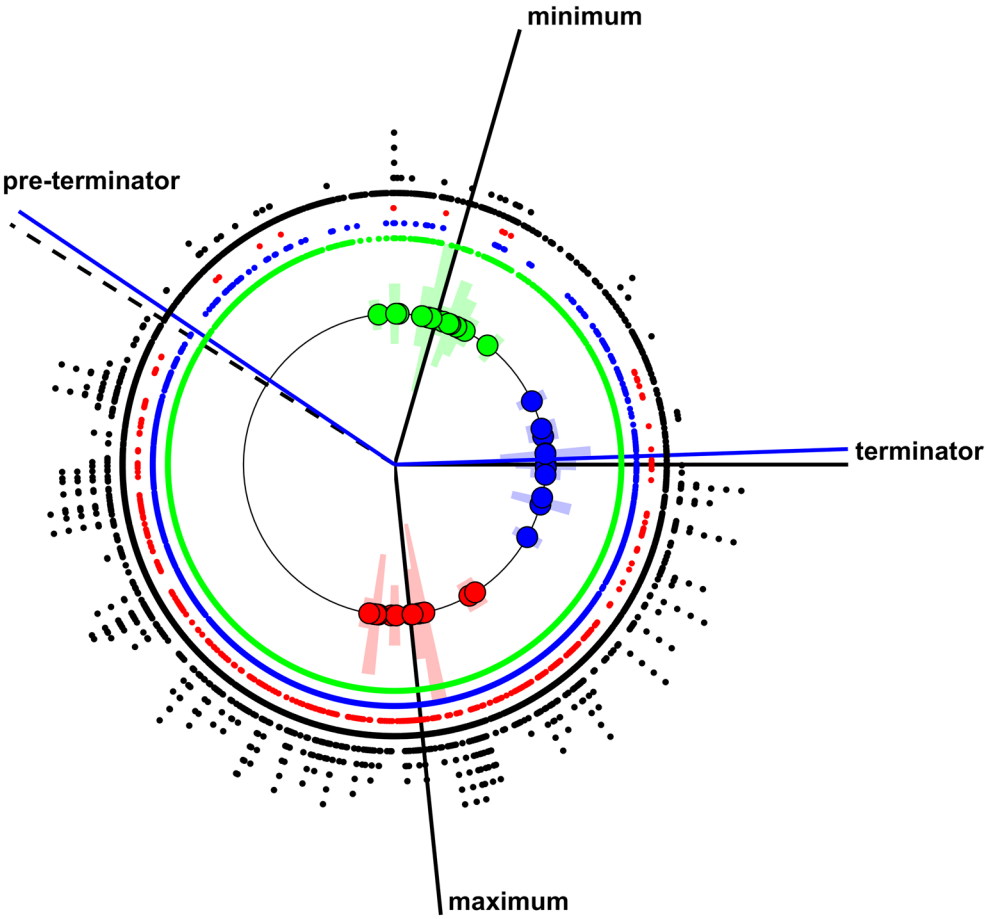

Figure 3. Solar cycle clock constructed as in Figure 2 to show geomagnetic activity. Black dots arranged on concentric circles where increasing radius indicates *aa* values which in any given day exceeded 100, 200, 300, 400, 500, and 600 nT. Red, blue, and green dots indicate days in which X-class, M-class, and C-class flares, respectively, occurred.

M-class, and C-class flare counts indicated by red, blue, and green histogram bars, respectively. In Figure 3, rings of red, blue, and green dots indicate (nonoverlapping) days in which X-class, M-class, and C-class flares, respectively, occurred. As we would expect, the occurrence of flares is modulated by the solar cycle. Daily F10.7 observations are overplotted for the full six-solar cycle record in Figure 2 (blue dots) and again are clearly ordered by the Sun clock.

To see to what extent the solar cycle clock orders geomagnetic activity, in Figure 3 we consider all 14 solar cycles of the 3 hr *aa* index (Mayaud, 1972). We aim to characterize extreme space weather events, but since *aa* is a coarse-grained measure (Bubenik & Fraser-Smith, 1977), its maximum excursions are not well resolved (Chapman et al., 2020). Rather than plot poorly resolved *aa* maximum values, we flag (nonoverlapping) calendar days in which any of the 3 hr *aa* index records in a given day exceeds a given threshold. The outer rings of Figure 2 (black dots) plot these flagged days with successively increasing radius for increasing threshold, $aa > 100$, 200, 300, 400, 500, and 600 nT. Radial "spokes" on this plot then indicate severe space weather events where multiple thresholds are simultaneously exceeded.

As expected, severe events are clustered more toward solar maximum. However the clock provides more quantitative detail on how the solar cycle orders solar coronal activity and severe space weather. We see that the average terminator time (phase) identifies a clear "switch on," that is, an increase in solar flare and severe space weather occurrence as we move from minimum to maximum in each cycle. Terminators have previously been identified solely from observations of solar coronal activity as the start time of each solar cycle; here we see the corresponding response in geomagnetic activity. Furthermore, as we move from maximum to minimum, there is a decrease or "switch off" in solar flare rates and severe space weather activity for

which we will introduce the terminology "pre-terminator." The "switch on" at the average terminator location occurs at a phase difference following average minimum of α=1.2769 radians (2.23 normalized years). We locate the pre-terminator at approximately the same phase difference preceding the average solar minimum on the solar cycle clock. We then see that between the pre-terminator and the terminator, there is a significantly lowered occurrence rate for severe storms; only one $aa > 500$ nT and a further two $aa > 300$ nT events occurred in the entire 151 year aa record. This identifies a specific "quiet interval" of the solar cycle which begins approximately $\alpha \simeq 2\pi/5$ (or 2.2 normalized years) before and ends approximately $\alpha \simeq 2\pi/5$ (or 2.2 normalized years) after the 18 cycle average phase of solar minimum as indicated by the blue lines on the clock; these can be seen to closely coincide with the terminator and pre-terminator. The 1903 storm that is associated with a quiet Sun outburst (Hayakawa et al., 2020) can be seen in Figure 3 just after the average terminator location outside this quiet interval. The terminator time, estimated from solar observations, then is potentially a tool to support operational decision making as it flags an imminent increase in the likelihood of more severe space weather activity. Since we have obtained the sunspot record analytic phase as a function of time, we can translate the terminator (activity "switch on") and pre-terminator (activity "switch off") phases into occurrence times. In Figure 1d, zero phase is that of the terminator average and we indicate in gray the range of phases $[-4\pi/5\ 0]$. These gray shaded regions then indicate the times of the quiet interval of each cycle. The sunspot number analytic phase can in principle be extrapolated forward in time, albeit with some uncertainty, to forecast when a specific phase will occur. This has been done for the terminator at the start of the next solar cycle (Leamon et al., 2020), and a similar procedure could also forecast when the "switch off" of activity will occur.

4. Quantifying Solar Cycle Modulation of the Level of Activity

To quantify solar coronal activity and occurrence rates of space weather of different severity, in Figure 4 we plot the information shown on the Sun clocks as histograms. The abscissa plots the range $[0\ 2\pi]$ of phase on the Sun clock as a normalized 11 year cycle, with Year zero at the average terminator occurrence time (phase). We form histograms of occurrences as counts in 3 month nonoverlapping bins within this 11 year cycle from the entire observational record for each quantity. Panels (a) and (b) plot the counts per 3 month bin of the number of days, during the full aa record since 1868, in which aa exceeds the above thresholds. Panels (c) and (d) count the number of C, M, and X flares per 3 month bin that were observed over the GOES catalog since 1975. Panel (e) overplots all individual records of F10.7; the index is available since 1947 giving six overplotted solar cycles.

In Figure 4 a gray shaded region indicates the quiet interval of the cycle, centered on the average location of solar minimum and demarcated by the pre-terminator (at −4.4 years) and terminator (at Year zero) as obtained from the Sun clock (Figures 2 and 3). The quiet interval clearly coincides with reduced occurrence rates for flares and severe space weather and low values of F10.7 solar radio flux. Indeed, only 12 of the 453 X-flares from the GOES flare catalog occurred when F10.7 was <90 sfu. Including weaker flares, only ∼4–6% of all X, M, or C-flares occurred in the quiet interval; the relative chance of a flare occurring in the quiet interval is roughly the same for all flare classes. Over the 14 solar cycles of the aa index record there were 19 occurrences of the most intense, $aa > 600$ nT events, and none of these occurred in the quiet interval. There were three events with $aa > 300$ nT, one of which reached $aa > 500$ nT in the quiet interval; ∼1–3% of all $aa \sim$ 300–500 nT days occurred in the quiet interval. This significantly modulates solar cycle averaged estimates of the occurrence rates of severe geomagnetic storms. If the occurrence rates were uniform across the solar cycle, a quiet interval of 4.4 years within an 11 year cycle would translate to 40% of all events occurring in the quiet interval. An overall number of C events in N years implies an average return period N/C, so that the 130 $aa > 300$ nT days seen in the entire aa record implies a return time of ~ 1.2 years. Given that approximately 4.4 out of 11 years are quiet, finding 3 $aa > 300$ nT events in quiet intervals translates to a quiet interval return period of ∼20 years for these events. Similarly, the active interval return period is $\sim$ 0.7 years. Counts and return periods are listed in supporting information Table S1.

From 14 cycles of aa index data we find that more moderate storm days are less strongly modulated by the solar cycle, with ∼21% of $aa > 100$ nT days occurring in the quiet interval. This is consistent with previous estimates based on the last five solar cycles. More moderate storms are more frequent, and hence an estimate of the solar cycle modulation of their occurrence rates can be attempted using observations over fewer solar cycles for which there are geomagnetic indices that are well resolved in amplitude so that individual storm peak disturbance values can be identified. Based on the five solar cycles of available D_{ST} observations,

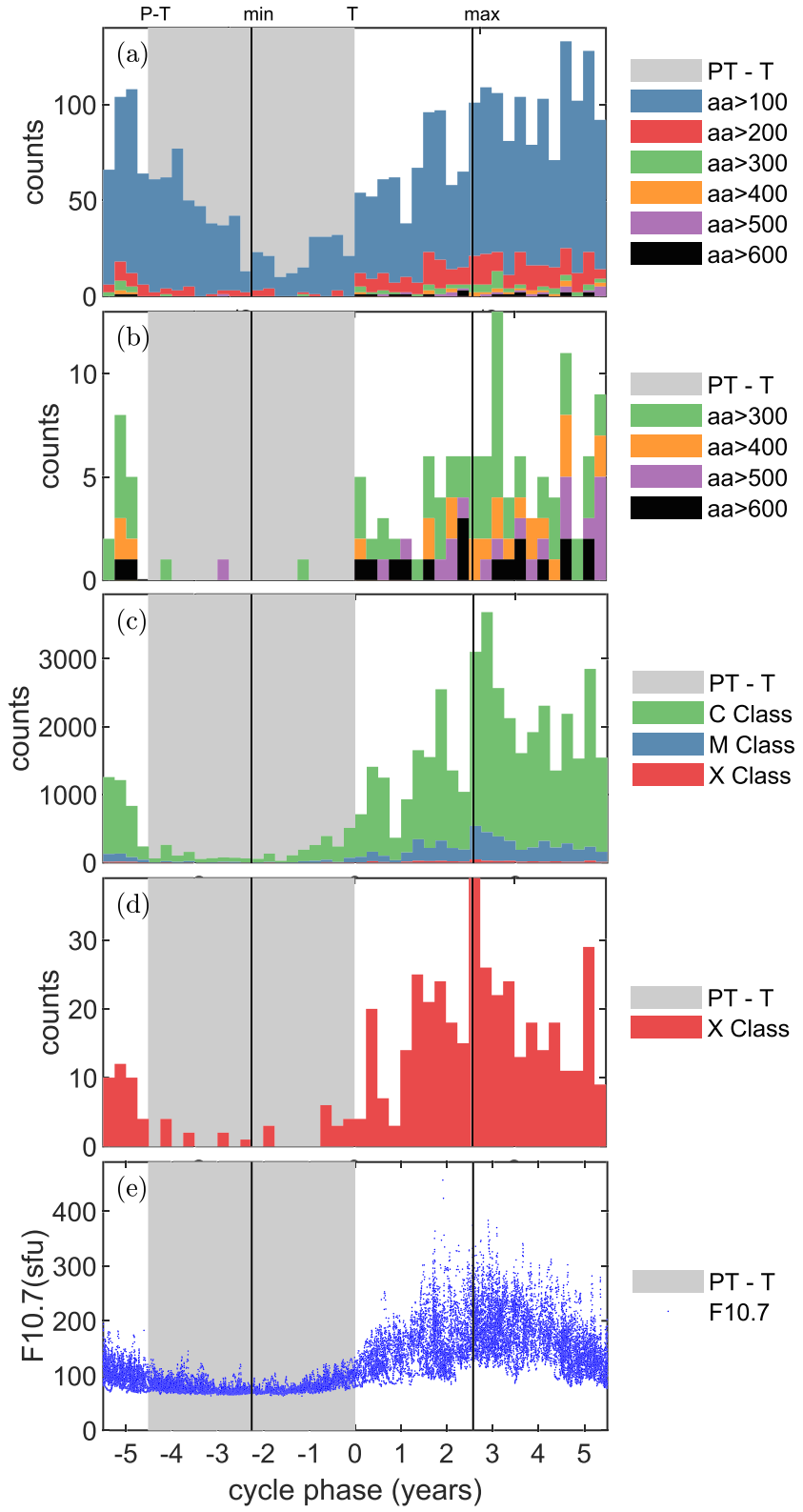

Figure 4. The abscissa plots the 2π in phase of a solar cycle on an 11 year time base with Year zero at the terminator. The average phases of solar maximum and minimum are indicated by vertical black lines. The average terminator and pre-terminator demarcate a quiet interval centered on minimum (shaded gray region). The ordinates are histogram counts of number of days in nonoverlapping 3-month-long bins in which (a) *aa* values exceeded 100, 200, 300, 400, 500, and 600 nT and (b) *aa* values exceeded 300, 400, 500, and 600 nT; (c) counts of C- and M-class and (d) X-class flares. Panel (e) plots the daily F10.7 versus analytic phase.

the occurrence rate of more moderate storms has been estimated to vary by a factor of 2–3 between solar maximum and minimum (Tsubouchi & Omura, 2007). Extrapolating distributions sorted by solar maximum and minimum to the most extreme events (Riley & Love, 2016) gives an occurrence likelihood that is more strongly solar cycle modulated, with 1.4% during solar minimum conditions and 28% in solar maximum conditions. This is again consistent with our findings; however, the analysis presented here does not require the assumption of any specific distribution or its extrapolation.

5. Conclusions

In summary, we constructed a new solar cycle clock by using a Hilbert transform of the daily sunspot number record to map the variable duration solar cycle onto a uniform $[0\ 2\pi]$ interval of analytic phase. We found this clearly identifies a ~4.4 year (normalized) quiet interval centered on solar minimum in a (normalized) 11 year cycle. The start and end of this quiet interval occur at specific analytic phases of the daily sunspot number which in principle are forecastable in real time by forward extrapolation of the relationship between time and analytic phase of the daily sunspot number record. Since F10.7 solar radio flux is also ordered by analytic phase, it could provide an additional signal with which to make this forecast.

Knowing when the next quiet interval will start and end has considerable implications for planning resilience of systems to the impacts of severe space weather events. Approximately 1–3% of all $aa > 300$ nT days in the *aa* record occurred in solar cycle quiet intervals giving a return period of ~ 20 years in quiet intervals and ~ 0.7 years in active intervals. Averaged over the solar cycle, the return period is ~ 1.2 years. The active interval return period differs from the solar cycle average by about a factor of 2. It is, however, significantly reduced during quiet intervals.

Across the *aa* record, we find that the occurrence rate of severe events is significantly more strongly solar cycle modulated than that of more moderate ones. Estimates of the likely occurrence rate based on more frequently occurring, moderate events may therefore underestimate the solar cycle modulation of more severe events. This pattern is not seen as strongly in the solar cycle modulation of solar flares where we find that the proportion that occurs in the quiet interval is roughly the same for C-, M-, and X-class flares. This may reflect the fact that more severe geomagnetic storms tend to be more directly correlated with flare activity, whereas more moderate storms can result from other drivers in the solar wind such as high-speed streams.

Data Availability Statement

The *aa* index data set is available from the International Service of Geomagnetic Indices (at http://isgi.unistra.fr/). The daily sunspot number data set is available from the SILSO, World Data Center—Sunspot Number and Long-term Solar Observations, Royal Observatory of Belgium, online Sunspot Number catalog (http://www.sidc.be/silso/datafiles). The dates of solar cycle maxima and minima are as determined from the smoothed sunspot number record by SILSO (http://www.sidc.be/silso/cyclesmm). The solar radio flux at 10.7 cm (the F10.7 index) is available since 1947 (at https://www.spaceweather.gc.ca/solarflux/sx-en.php). The GOES X-ray Flare data set is available through the NOAA National Geophysical Data Center (NGDC) (https://www.ngdc.noaa.gov/stp/space-weather/solar-data/solar-features/solar-flares/x-rays/).

Acknowledgments
The results presented in this paper rely in part on geomagnetic indices calculated and made available by ISGI Collaborating Institutes from data collected at magnetic observatories. We acknowledge the involved national institutes, the INTERMAGNET network (www.intermagnet.org), and ISGI (isgi.unistra.fr). We thank the World Data Center for Geomagnetism, Kyoto. We thank the World Data Center SILSO, Royal Observatory of Belgium, Brussels, for provision of sunspot data. S. C. C. acknowledges a Fulbright-Lloyd's of London Scholarship and AFOSR Grant FA9550-17-1-0054 and ST/P000320/1. S. C. C., N. W. W., and R. J. L. appreciate the support of the HAO Visitor Program. R. J. L. acknowledges support from NASA's Living With a Star Program.

References

Babcock, H. W. (1961). The topology of the Sun's magnetic field and the 22-year cycle. *Astrophysical Journal*, *133*, 572.

Baker, D. N., & Lanzerotti, L. J. (2016). Resource letter SW1: Space weather. *American Journal of Physics*, *84*, 166. https://doi.org/10.1119/1.4938403

Bartels, J., Heck, N. H., & Johnston, H. F. (1939). The three-hour-range index measuring geomagnetic activity. *Journal of Geophysical Research*, *44*, 11. https://doi.org/10.1029/TE044i004p00411

Boashash, B. (1992). Estimating and interpreting the instantaneous frequency of a signal. I. Fundamentals. *Proceedings of the IEEE*, *80*(4), 520–568.

Bubenik, D. M., & Fraser-Smith, A. C. (1977). Evidence for strong artificial components in the equivalent linear amplitude geomagnetic indices. *Journal of Geophysical Research*, *82*, 2875.

Chapman, S. C., Horne, R. B., & Watkins, N. W. (2020). Using the *aa* index over the last 14 solar cycles to characterize extreme geomagnetic activity. *Geophysical Research Letters*, *47*, e2019GL086524. https://doi.org/10.1029/2019GL086524

Chapman, S. C., Lang, P. T., Dendy, R. O., Giannone, L., & Watkins, N. W. (2018). ASDEX upgrade team, control system-plasma synchronization and naturally occurring edge localized modes in a tokamak. *Physics of Plasmas*, *25*, 62511. https://doi.org/10.1063/1.5025333

Chapman, S. C., Watkins, N. W., & Tindale, E. (2018). Reproducible aspects of the climate of space weather over the last five solar cycles. *Space Weather*, *16*, 1128–1142. https://doi.org/10.1029/2018SW001884

Elvidge, S., & Angling, M. J. (2018). Using extreme value theory for determining the probability of Carrington-like solar flares. *Space Weather*, *16*, 417–421. https://doi.org/10.1002/2017SW001727
Gabor, D. (1946). Theory of communication. *Journal IEE (London)*, *93*(3), 429–441.
Hapgood, M. (2019). The great storm of May 1921: An exemplar of a dangerous space weather event. *Space Weather*, *17*, 950–975. https://doi.org/10.1029/2019SW002195
Hathaway, D. H. (2015). The solar cycle. *Living Reviews in Solar Physics*, *12*, 4. https://doi.org/10.1007/lrsp-2015-4
Hayakawa, H., Ribeiro, P., Vaquero, J. M., Gallego, M. C., Knipp, D. J., Mekhaldi, F., et al. (2020). The extreme space weather event in 1903 October/November: An outburst from the quiet Sun. *The Astrophysical Journal Letters*. https://doi.org/10.3847/2041-8213/ab6a18
Leamon, R. J., McIntosh, S. W., Chapman, S. C., & Watkins, N. W. (2020). Timing terminators: Forecasting sunspot cycle 25 onset. *Solar Physics*, *295*, 36. https://doi.org/10.1007/s11207-020-1595-3
Lockwood, M., Owens, M. J., Barnard, L., Scott, C. J., Usoskin, I. G., & Nevanlinna, H.(2016). Tests of sunspot number sequences: 2. Using geomagnetic and auroral data. *Solar Physics*, *291*, 2811–2828. https://doi.org/10.1007/s11207-016-0913-2
Lockwood, M., Owens, M. J., Barnard, L. A., Scott, C. J., Watt, C. E., & Bentley, S. (2018). Space climate and space weather over the past 400 years: 2. Proxy indicators of geomagnetic storm and substorm occurrence. *Journal of Space Weather and Space Climate*, *8*, A12. https://doi.org/10.1051/swsc/2017048
Lockwood, M., Owens, M. J., Barnard, L., & Usoskin, I. G. (2016). Tests of sunspot number sequences: 3. Effects of regression procedures on the calibration of historic sunspot data. *Solar Physics*, *291*, 2829–2841. https://doi.org/10.1007/s11207-015-0829-2
Marple, S. L. (1999). Computing the discrete-time analytic signal via FFT IEEE. *Transactions on Signal Processing*, *47*, 2600–2603.
Mayaud, P.-N. (1972). The *aa* indices: A 100 year series characterizing the magnetic activity. *Journal of Geophysical Research*, *77*, 6870.
Mayaud, P. N. (1980). Derivation, meaning, and use of geomagnetic indices, *Geophysical Monograph Series* (Vol. 22). Washington, D.C: AGU. https://doi.org/10.1029/GM022
McIntosh, S. W., & Leamon, R. J. (2014). On magnetic activity band overlap, interaction, and the formation of complex solar active regions. *Astrophysical Journal Letters*, *796*, L19.
McIntosh, S. W., Leamon, R. J., Egeland, R., Dikpati, M., Fan, Y., & Rempel, M. (2019). What the sudden death of solar cycles can tell us about the nature of the solar interior. *Solar Physics*, *294*(7), 88. https://doi.org/10.1007/s11207-019-1474-y
McIntosh, S. W., Wang, X., Leamon, R. J., & Scherrer, P. H. (2014). Identifying potential markers of the Sun's giant convective scale. *Astrophysical Journal Letters*, *784*, L32.
Oughton, E. J., Skelton, A., Horne, R. B., Thomson, A. W. P., & Gaunt, C. T. (2017). Quantifying the daily economic impact of extreme space weather due to failure in electricity transmission infrastructure. *Space Weather*, *15*, 65–83.
Palŭs, M., & Notovná, D. (1999). Sunspot cycle: A driven nonlinear oscillator? *Physical Review Letter*, *83*, 3406.
Riley, P. (2012). On the probability of occurrence of extreme space weather events. *Space Weather*, *10*, S02012. https://doi.org/10.1029/2011SW000734
Riley, P., & Love, J. J. (2016). Extreme geomagnetic storms: Probabilistic forecasts and their uncertainties. *Space Weather*, *15*, 53–64. https://doi.org/10.1002/2016SW001470
Russell, C. T., Jian, L. K., & Luhmann, J. G. (2019). The solar clock. *Reviews Geophysics*. https://doi.org/10.1029/2019RG000645
Sheeley, N. R., Wang, Y.-M., & Harvey, J. W. (1989). The effect of newly erupting flux on the polar coronal holes. *Solar Physics*, *119*, 323.
Silbergleit, V. M. (1996). On the occurrence of geomagnetic storms with sudden commencements. *Journal of Geomagnetism and Geoelectricity*, *48*, 1011.
Silbergleit, V. M. (1999). Forecast of the most geomagnetically disturbed days. *Earth Planets Space*, *51*, 19.
Siscoe, G. L. (1976). On the statistics of the largest geomagnetic storms per solar cycle. *Journal of Geophysical Research*, *81*, 4782.
Tapping, K. F. (2013). The 10.7 cm solar radio flux (F10.7). *Space Weather*, *11*, 394–406. https://doi.org/10.1002/swe.20064
Thomson, A. W. P., Dawson, E. B., & Reay, S. J. (2011). Quantifying extreme behaviour in geomagnetic activity. *Space Weather*, *9*, S10001. https://doi.org/10:1029/2011SW000696
Thomson, A. W. P., Gaunt, C. T., Cilliers, P., Wild, J. A., Opperman, B., McKinnell, L.-A., et al. (2010). Present day challenges in understanding the geomagnetic hazard to national power grids. *Advance Space Research*, *45*, 1182–1190. https://doi.org/10.1016/j.asr.2009.11.023
Tsubouchi, K., & Omura, Y. (2007). Long-term occurrence probabilities of intense geomagnetic storm events. *Space Weather*, *5*, S12003. https://doi.org/10.1029/2007SW000329
Tsurutani, B. T., Gonzalez, W. D., Gonzalez, A. L. C., Guarnieri, F. L., Gopalswamy, N., Grande, M., et al.(2006). Corotating solar wind streams and recurrent geomagnetic activity: A review. *Journal of Geophysical Research*, *111*, A07S01. https://doi.org/10.1029/2005JA011273
Tsurutani, B. T., Gonzalez, W. D., Lakhina, G. S., & Alex, S. (2003). The extreme magnetic storm of 1–2 September 1859. *Journal of Geophysical Research*, *108*(A7), 1268. https://doi.org/10.1029/2002JA009504
Vedder, J. D., & Tabor, J. L. (1992). Solar F10.7 radiation: A short-term statistical model. *Journal of Spacecraft and Rockets*, *29*, 76. https://doi.org/10.2514/3.26316
Yermolaev, Y. I., Lodkina, I. G., Nikolaeva, N. S., & Yermolaev, M. Y. (2013). Occurrence rate of extreme magnetic storms. *Journal of Geophysical Research: Space Physics*, *118*, 4760–4765. https://doi.org/10.1002/jgra.50467